Journal of Colloid and Interface Science 333 (2009) 628–634

Contents lists available at ScienceDirect

Journal of Colloid and Interface Science

www.elsevier.com/locate/jcis

Nanotribology, standard friction, and bulk rheology properties compared for a Brij microemulsion

M. Graca [a], J.H.H. Bongaerts [b], J.R. Stokes [b,c], S. Granick [a,*]

[a] Department of Materials Science and Engineering, University of Illinois, Urbana, IL 61801, USA
[b] Unilever Corporate Research, Colworth Science Park, Sharnbrook, MK44 ILQ, UK
[c] University of Queensland, Division of Chemical Engineering, Brisbane Qld 4072, Australia

ARTICLE INFO

Article history:
Received 25 November 2008
Accepted 24 January 2009
Available online 29 January 2009

Keywords:
Microemulsion
Nanotribology
Friction
Rheology
Brij

ABSTRACT

A microemulsion consisting of Brij 96, glycerol (co-surfactant), oil, and water was compared as concerns deformations in a surface forces apparatus whose surface where rendered hydrophobic by coating with a monolayer of condensed OTE (octadecyltriethoxysilane), as concerns tribology of the conventional kind during sliding between hydrophobic PDMS surfaces, and as concerns bulk rheology. In the bulk, light scattering characterization showed swollen spherical micelles with a 13 nm diameter. When squeezed to form thinner films than this, the effective viscosity measured rose by orders of magnitude. It appears that thin films in the range of thickness 13 to 7 nm are comprised of deformed micelles and that confinement to thinner films expels micelles with concomitant even more drastic structural deformation of the remaining micelles, until the thinnest films retain only adsorbed surfactant. Tentatively, this may explain why the friction response then became similar to that of surfactant itself [M. Graca, J.H.H. Bongaerts, J.R. Stokes, S. Granick, J. Colloid Interface Sci. 315 (2007) 662]. These measurements are considered to be the first comparison of microemulsion rheology in the bulk and in nanometer-thick films.

1. Introduction

Microemulsions are thermodynamically stable isotropic dispersions consisting of water and oil, stabilized (often in combination with a co-surfactant) by an interfacial film of surfactant molecules. Their low viscosity and other distinctive properties afford them wide use in specialty chemical, pharmaceutical, petrochemical, personal care, food and many other applications. As their applications commonly involve deformation, much is known about their bulk rheological properties [1]. However, during lubrication, microemulsions are confined into narrow spaces whose thickness may become comparable to those of the micelles themselves. Little is known about the mechanical responses of such systems, most likely because of the difficulties to measure their properties. In fact, multi-phase complex fluids in general have not been studied much at all in nano-scale confinement, even though this is a subject of considerable relevance to many everyday processes. It is natural to anticipate a structure different from that characteristic of the bulk microemulsion, and correspondingly a different mechanical response. This is the topic of the current study.

Motivating this study is the hypothesis that microemulsions in confined geometries, at spacing comparable to those of the micellar structure itself, may be central to sensory applications—especially to so-called "in-use feel" of personal care products and "mouthfeel" of food products—as well as to the deposition of components from within the micelles. Transparent to the eye, in the range of oil composition considered in this paper, microemulsions consist of swollen oil-containing micelles with diameter in the range of 5–100 nm. More generally, they can also be comprised of lamellar phases and can adopt bicontinuous oil/water (o/w) structure; moreover, in addition to the oil/water systems considered in this paper, they can also involve polymers [2,3], gels, and charged surfactants and co-surfactants of more than a single charge [4–6]. Whereas the highly-concentrated systems that form bicontinuous structures display pronounced shear thinning [6] in their bulk rheological response, this is not so of the spherical micellar structures of concern in this study, whose bulk rheology has been found to be similar to that of hard spheres [1].

This study is the sequel to an earlier study by the same authors [7] in which, to set the stage for the present study, we studied the friction of surfactants adsorbed at the same types of hydrophobic surfaces studied here. In that study, a series of nonionic poly(oxyethylene) surfactants (Tween-20, Tween-40, Tween-60 and Tween-80) were allowed to adsorb from aqueous solution onto atomically smooth hydrophobic substrates composed of a condensed monolayer of octadecyltriethoxysilane (OTE) (water contact angle $\theta > 110°$). That study showed that these surfactants adsorbed to form a robust separating layer whose lubricating prop-

* Corresponding author.
E-mail address: sgranick@uiuc.edu (S. Granick).

0021-9797/$ – see front matter
doi:10.1016/j.jcis.2009.01.051

erties were the same for all alkyl chain lengths and characterized by a shear stress of approximately 3 MPa with minimal dependence on shear rate. In the present study, microemulsions were confined between hydrophobic surfaces prepared in the same way. Furthermore, in this paper we compare nanotribology measurements made in a surface forces apparatus with bulk rheology and friction studies. For this purpose the tribometer, adapted for soft-contact friction measurements, was equipped with hydrophobic poly(dimethylsiloxane) (PDMS) substrates showing a water contact angle of 100°.

2. Materials and methods

2.1. Materials

A non-ionic surfactant, Brij 96 (polyoxyethylene 10 oleoyl ether), was chosen because of ease of microemulsion formation [8], as well as widespread availability, applicability, and low toxicity or irritation potential [9]. It was mixed in the proportions given below with glycerol (co-surfactant) to influence the optimal head group area and a medium chain triglyceride oil (MCT) at high temperature, combined with hot water (∼90 °C), and brought to room temperature whilst stirring to form small micelles. This kind of microemulsion formation is called the phase inversion temperature (PIT) method and is particularly useful when using ethoxylated non-ionic amphiphiles. When heated, these ingredients form a water-in-oil (w/o) emulsion above the critical temperature, the PIT. At the PIT, the droplet size and the interfacial tension reach a minimum, and during cooling a stable oil-in-water (o/w) microemulsion forms, consisting of spherical swollen micelles [10].

The components were mixed in the following ratio: Brij 96 4.5%, glycerol 1.5%, MCT 2%, water 92%. Not only is the method of preparation important (based on the phase diagram), but also the ratio of a surfactant/co-surfactant to oil, which should be kept at 3:1. Brij 96V was purchased from Fluka. Glycerol (99.5+% ACS reagent (water ⩽0.5%)) was purchased from Sigma-Aldrich. MCT oil (a lipid fraction of coconut oil consisting primarily of triglycerides of C_8 and C_{10} saturated fatty acids) was purchased from Novartis Medical Nutrition. Nano-pure deionized water was used in all sample preparations. The size of the spherical micelles in the microemulsion was measured using dynamic light scattering (Zetasizer Nano ZS, Malvern Instruments Ltd.) and found to be ∼13.7 nm (Fig. 2). The obtained normal emulsion (E) had a typical milky color and an emulsion droplet size of ∼5 μm.

For the fabrication of OTE monolayers, N-octadecyltriethoxysilane (OTE) was purchased from Hüls America, Inc. In the literature, as different groups have reported variable experiences when it comes to making OTE monolayers of good quality [11–14], it is clear that the resulting monolayers depend highly on details of the experimental protocol. A detailed discussion of the experimental protocols that have been found in this laboratory to be most effective will be presented presently. Briefly, previous studies from this laboratory showed that the packing density and degree of crystallinity in well-prepared monolayers are comparable to those of an LB (Langmuir–Blodgett) film of barium stearate [15]. Furthermore, the thickness of two OTE monolayers in contact in air, measured in a surface forces apparatus, is 51 ± 3 Å relative to mica–mica contact [16]. In order to form monolayers of low roughness, we found it necessary to purify the as-purchased chemical by vacuum distillation at 300 m Torr, at which the liquid was found to boil at 165 °C. Other procedures of OTE monolayer formation were essentially as described earlier by this laboratory [15,17] with the modifications described below. The surface energy of the resulting methyl terminated surfaces is known to be 22 mJ/m^2 [15,17].

Tetrahydrofuran (THF), HPLC/spectrophotometric grade, was purchased from Fischer Scientific and used as the solvent for hydrolyzing OTE before monolayer formation. The prehydrolysis solution was a mixture of 0.21 g distilled OTE and 0.125 g 1.3 M HCl, diluted with THF to 25 mL total in a volumetric flask. The solution was held at room temperature for a minimum of 36 h and then diluted with cyclohexane (0.6 g of prehydrolysis solution dissolved in 10 g of cyclohexane) forming the so-called dipping solution. OTE was coated onto mica sheets by immersion in the dipping solution for 35 min. Immediately after removal from the dipping solution the samples were rinsed in a sequence of solvents: cyclohexane followed by 2-propanol and acetone, followed by ultrasonication in each for 3 min to remove the excess non-adsorbed OTE, micelles or other polymerized clusters from the substrate. In the final monolayer formation step they were baked in a vacuum oven (125 °C) for 2 h. Cyclohexane, 2-propanol and acetone were purchased from Sigma-Aldrich, HPLC or spectrophotometric grade, and used as received. The muscovite mica (V-4 grade) was freshly cleaved manually.

The poly(dimethylsiloxane) (PDMS) used to form the tribopair in the tribometer was purchased from Dow Corning, and was a two-component silicone elastomer kit (Sylgard 184). Curing agent and a base were used in a ratio of 1:10. The liquid PDMS was coated into the mold of a sphere and disk respectively and cured for 2 h in the oven at 55 °C. The ready components were removed from the mold after cooling overnight. The PDMS ball ended up with a radius of 0.95 cm and the PDMS disk was of radius 23 mm and a thickness of 4 mm. Young's modulus of this material is $E = 2.4$ MPa. More detailed tooling preparation is described elsewhere [18].

2.2. Surface Forces Apparatus (SFA)

The home-built surface forces apparatus in the University of Illinois laboratory, equipped for dynamical viscoelastic measurements in oscillatory shear, has been described at length previously [19,20]. The output voltage and phase were measured by digital lock-in amplifier (Stanford Research Systems SR850).

The geometry consists of two molecularly-smooth cylindrical mica surfaces with a curvature radius $R \approx 2$ cm, arranged in crossed cylinder geometry. The surface separation was measured by multiple-beam interferometry and detected by CCD camera using standard techniques with an accuracy of 1–2 Å. In circumstances where the cylindrical sheets of mica were undeformed by the normal forces squeezing them together (relatively large surface–surface separations), the shear forces were normalized by an effective contact area; this is determined by calculating, as described in earlier studies from this laboratory [19], the contact diameter with respect to the measured contact diameter at the maximum applied normal force, assuming a Hertzian contact, which is a reasonable assumption when one recalls that it is the glue under the mica that deforms under the action of normal pressure [19]. In the measurements described below, the normal load pressing the sheets of mica together caused the apex of each sheet to deform, producing a locally-flattened contact area in which the sheets of mica were parallel to within the experimental uncertainty of thickness measurement. The contact diameter for the thinnest films was calculated from the flattened tip of the interference fringes taking into account the lateral magnification of the focusing mechanism. The shear forces were normalized by the measured contact area to give the shear stress.

The muscovite mica used in the measurements (V-4 grade), was first cleaved and silvered on the backside using standard techniques, then attached to cylindrical quartz lenses using a thermosetting epoxy glue (Norland Electronic Adhesive). Such prepared lenses were then coated with an OTE monolayer as described above. In the findings described below, surface–surface separation

refers to thickness after subtracting the calibrated thickness of two OTE monolayers in air.

Oscillatory shear deformation was accomplished by mounting the top surface to a small boat rigidly attached to two piezoelectric bimorph strips, for which the dominant motion is bending. The other ends of the bimorphs were fixed in a base support by an epoxy glue. To increase flexibility, each bimorph was lengthened at one end with a short strip of more flexible steel spring by gluing the two. Shear was induced when a voltage difference applied between the two sides of one of the bimorphs bent it. The resulting displacement was transferred to the other bimorph through the rigidly attached boat inducing a voltage difference between the two sides. The comparison of this output voltage when the surfaces are apart, called the calibration output, with that when the surfaces were in contact with the intervening fluid gave information about the response of the fluid to the applied shear. Viscoelastic forces from the confined fluid resist the applied shear motion and result in amplitude attenuation and phase shift in the thin-film situation.

The methods to infer force and motion from voltage induced in piezoelectric bimorphs were described previously [16,19,20]. In brief, the mechanical and the electrical characteristics of the shear device, together with the mechanical behavior of the intervening fluid, were previously modeled and we derived expressions relating the measured amplitude attenuation and the phase shift to the apparent dynamic viscosity and the elastic modulus of the liquid—the mechanical model replaces the device, glue and the liquid with a combination of effective masses, springs and dashpots. Simply put, a complex impedance, $Z_D = k_D + i\omega b_D$, can be assigned to the device, which responds like an underdamped forced harmonic oscillator when a voltage is applied to the input terminals. Here the real part of the impedance represents the equivalent spring constant of the device, a combination of the spring constants of the bimorphs and the leaf springs. The imaginary part is due to dissipation in the system, mostly caused by the adhesive that holds the bimorphs to the leaf springs. In this configuration the applied stress is split into two, between the device and the combination of glue and liquid. The resulting displacement is the sum of the displacement of the glue and the displacement of the liquid. Earlier studies from this laboratory analyzed the glue displacement in detail and showed that it does not change with time [16,19].

Each experiment began by bringing the OTE-coated mica lenses into contact in air to calibrate the thickness by interferometry and to confirm cleanliness and smoothness of the monolayer surfaces. The surfaces were imaged using standard methods of optical interferometry [21] to give the surface separation and contact (~45 μm diameter) at the apex of the flattened contact under high normal load. By measuring the oscillatory deflection amplitude and phase in response to an oscillatory shear driving force, effective viscous and elastic shear moduli at the frequency of the drive signal were measured using these piezoelectric techniques [16,19,20].

For subsequent analysis, the shear forces were normalized by contact area to give stress, and stress was normalized by the film thickness to give the *effective* shear moduli. For this purpose we took the elastic and viscous force constants and normalized them by the effective contact area, A_{eff}, and film thickness, D, to give the effective shear moduli in and out of phase with the drive, G'_{eff} and G''_{eff}, respectively. Here A_{eff} was estimated as described by a Hertzian contact (see above). Moreover, the dynamic viscosity that quantifies energy dissipation was defined in the traditional rheological way as the loss modulus normalized by oscillatory frequency. Specifically,

$$G'_{\text{eff}}(\omega) = \left[\left(f_{\text{elastic}}(\omega)/d\right)\right][D/A_{\text{eff}}], \tag{1}$$

$$G''_{\text{eff}}(\omega) = \left[\left(f_{\text{viscous}}(\omega)/d\right)\right][D/A_{\text{eff}}], \tag{2}$$

$$\eta'_{\text{eff}}(\omega) \equiv G''_{\text{eff}}(\omega)/\omega, \tag{3}$$

where ω is the radian oscillation frequency and the symbol d refers to the shear amplitude in oscillatory deformation. The elastic force constant is $f_{\text{elastic}}(\omega)/d$ and the viscous force constant is $f_{\text{viscous}}(\omega)/d$. Moreover, it is known that when the amplitude of oscillatory deflection greatly exceeds the film thickness, the viscous response depends not on frequency but on the maximum velocity during the cycle of oscillation, which is the product of frequency and oscillatory shear amplitude [16,19]. Normalizing velocity by film thickness gives the effective shear rate.

Normal loads corresponding to 3 MPa pressure were used to produce the thinnest films, at which the oscillatory shear frequency was swept over the range 1.3 to 287 Hz and displacement amplitude up to 150 nm to produce the range of effective shear rates in the findings described below.

Whereas conventional measurements of linear viscoelastic response concern rheological response that is strictly at the same frequency as the drive frequency, as strains increase the dynamics of response become nonlinear and higher odd-order harmonics are generated (the even-order harmonics are zero because the stress is an odd function of strain). Detailed considerations described previously [16] show that the energy dissipated over one complete cycle of oscillation is determined by $G''_{\text{eff}}(\omega)$ where this quantity is measured at the drive frequency, i.e. a cancellation of higher-order terms signifies that they fail to contribute. With these considerations in mind, in this study we report values of elastic responses only for experiments where the deformation amplitude was comparable to or smaller than the film thickness; when the deformation exceeds the film thickness, only the effective viscosity is reported.

Building on these nano-rheological measurements, within the experimental platform of the surface forces apparatus the interaction force between the two surfaces were measured as a function of surface separation (film thickness) as the two surfaces were being brought into contact. The force in the direction normal to the surfaces, F, was calculated from deflection of the spring (spring constant, $k = 1160$ N/m) that supported the lower surface. The force F was normalized by the geometric mean of the radii of curvature of the crossed cylinders R (~2 cm), since the value F/R is proportional, by the Derjaguin approximation, to the interaction energy per unit area between two parallel plates for non-deformed surfaces. The voltage constant, displacement per output voltage, was 343 nm/V. Experiments were conducted at room temperature, 23–24 °C.

Both static and dynamic measurements began by bringing OTE coated mica substrates into hard contact with an applied pressure of 3 MPa, checking smoothness and cleanness, and calibrating the equipment before separating the surfaces and filling the gap with microemulsion. In the case of sliding shear studies, all measurements were carried out in hard contact. In the case of normal forces studies, a microemulsion sample was first brought into hard contact, then separated to obtain a thick film (~1 μm), and finally squeezed back to a nm-thick thin film.

2.3. Controlled strain rheometer

Viscoelastic properties of thin films of microemulsions obtained using the SFA were compared with bulk properties measured at Unilever, UK, at 35 °C on a controlled strain rheometer (ARES, Rheometric Scientific, Piscataway, NJ, USA). A cone and plane geometry with a 50 mm diameter cone of angle 0.02 radians was used to ensure a constant shear rate in the sample. All experiments were repeated three times and averaged. The sample was sheared at a rate of 1–630 s^{-1}, and the viscosity determined as a function of applied shear rate.

2.4. Mini Traction Machine (MTM)

Macroscopic tribological measurements were performed at Unilever U.K. on a modified commercial mini traction machine tribometer (MTM, PCS Instruments Ltd., London, UK). The rubbing contact occurs between a poly(dimethylsiloxane) (PDMS) ball with a radius 0.95 cm and a disk with a radius of 23 mm and a thickness of 4 mm. Both surfaces are independently driven by different motors, so the entrainment speed and sliding speed can be varied independently. All the experiments were carried out at a temperature of 35 °C and sliding friction was measured over a wide entrainment speed range at a slide-to-roll ratio of 50%. The load in all measurements was 1 N, which gave a contact diameter of 2.4 mm and an average pressure of 0.22 MPa, which is 1 order of magnitude lower than in the SFA experiment. The velocity-dependent friction measurements were repeated three times to check reproducibility and no changes were observed in friction data indicating that the rubbing contact did not wear. The highest speed applied was $U = 2.5$ m/s, and the lowest possible entrainment speed was limited by equipment and was $U = 1 \times 10^{-3}$ m/s. More detailed information about the equipment is available in Ref. [18].

3. Results and discussion

3.1. Perspective from bulk rheology

Fig. 1 compares photographs of the Brij 96 surfactant in water solution (S), emulsion (E) and microemulsion (M) for the same ratio of the components. Whereas the Brij 96/water solution (S) and the microemulsion (M) are transparent (with a slight bluish shade for the microemulsion), the normal emulsion is opaque. Fig. 2 shows the narrow distribution of micelle size in the microemulsion, obtained from dynamic light scattering.

The bulk rheological properties of the microemulsion are shown in Fig. 3, where viscosity (η) and stress are plotted as functions of shear rate. The viscosity (η) is constant, $\eta = 1.46$ mPa s. This is only marginally larger than for water, for which $\eta = 0.725$ mPa s at 35 °C. As viscosity is constant, shear stress increases in direct proportion to shear rate, reaching 0.9 Pa for the fastest shear speed applied. Experiments of this kind also showed Newtonian behavior for emulsion (E) and surfactant/water solution (S) (not shown here). None of the samples demonstrated a yield stress. Taken together, these experiments showed a simple rheological behavior; no relaxation processes slower than the smallest inverse shear rate.

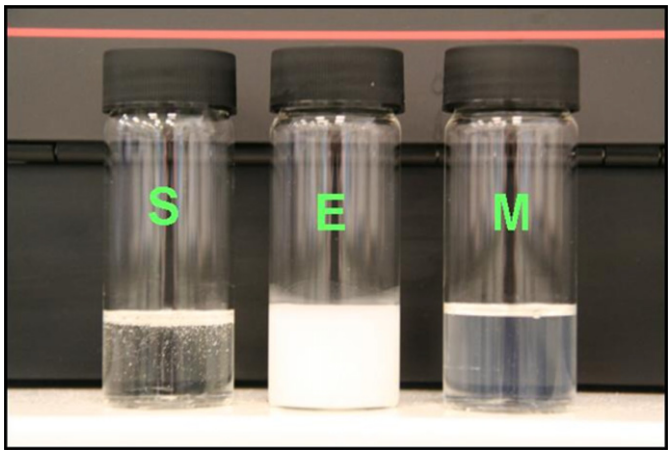

Fig. 1. Photographs of the Brij 96 based mixtures: (S) water solution, (E) emulsion, (M) microemulsion. The ratio of surfactant to water is the same, 20 to 1, for all three samples. The emulsion and microemulsion have the same composition: surfactant (Brij 96), co-surfactant (glycerol), MCT oil, and water, in the ratio 4.5%, 1.5%, 2% and 92%, respectively.

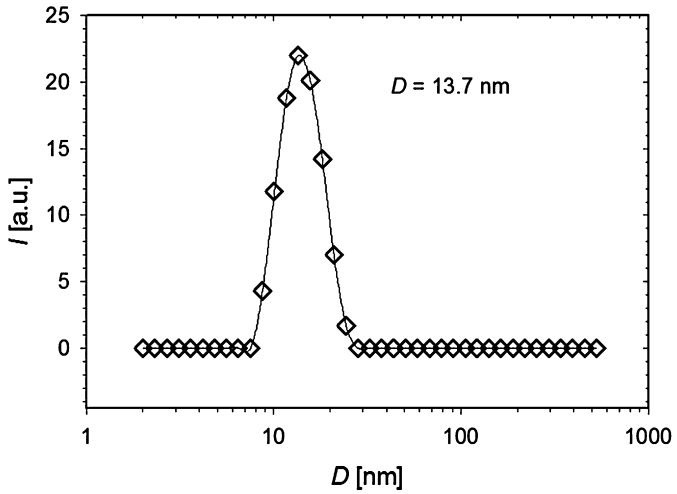

Fig. 2. Distribution of micelle diameter (D) determined by dynamic light scattering (Zetasizer Nano ZS from Malvern Instruments, Ltd.). Relative abundance is plotted against logarithmic D and the mean value is $D = 13.7$ nm.

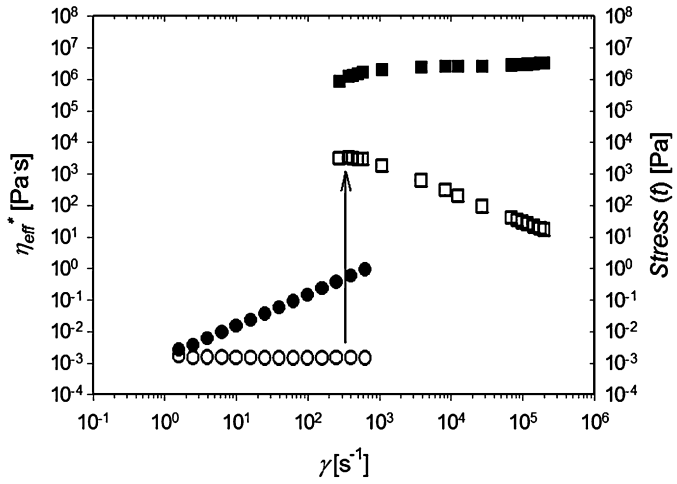

Fig. 3. Effective viscosity (left hand ordinate) and shear stress (right axis) are plotted against effective shear rate on log–log scales for the microemulsion described in the text. Effective viscosity is denoted by the open symbols. Stress is denoted by the solid symbols. Bulk measurements (circles) were taken using a commercial rheometer as described in the text. Thin-film measurements on films compressed by a normal pressure of 3 MPa (squares) to a thickness of 4.4 nm were taken using a surface forces apparatus as described in the text. Both macro and nano measurements employed hydrophobic surfaces, as described in the text.

3.2. Nanometer-sized films

Included in Fig. 3 is the comparison of these same parameters measured after confining this same microemulsion under a pressure of 3 MPa to the thickness of 4.4 ± 0.3 nm. Owing to instrumental limitations, most of these thin-film experiments refer to higher shear rates than could be measured in bulk experiments, but there is a small region of overlap in shear rate. At the smallest shear rates (100–600 s^{-1}) shear stress increases in direct proportion to shear rate; the effective viscosity is constant at 5×10^3 Pa s. At even higher shear rates the shear stress rises to a level where it is independent of shear rate, 3×10^6 Pa; in this region, the effective viscosity consequently diminishes in direct proportion to shear rate. The shear stress of the thin film exceeds that of the bulk sample by orders of magnitude and, beyond the shear rate of 1×10^3 s^{-1}, becomes decidedly nonlinear in its response to variations of the shear rate.

The linear viscoelastic behavior was also of interest. For comparison with the experiments summarized in Fig. 3, for which the

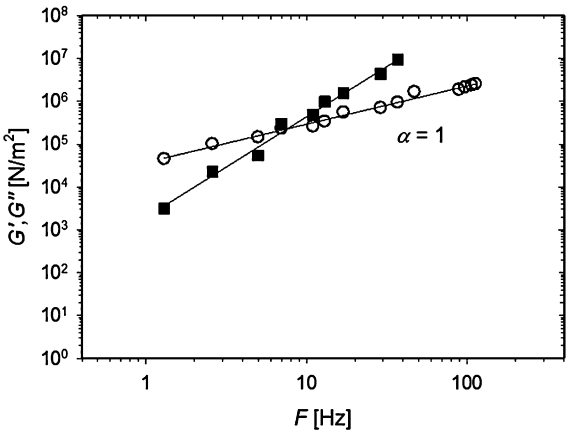

Fig. 4. Log–log plot versus angular frequency of the effective storage modulus, $G'(\omega)$ (solid squares) and loss modulus, $G''(\omega)$ (open circles), for a microemulsion film of Brij 96 compressed by a normal pressure of MPa to thickness 4.4 nm. Note that the response is predominantly viscous below 300 s^{-1} and predominantly elastic above this shear rate. Hydrophobic surfaces were employed, as described in the text.

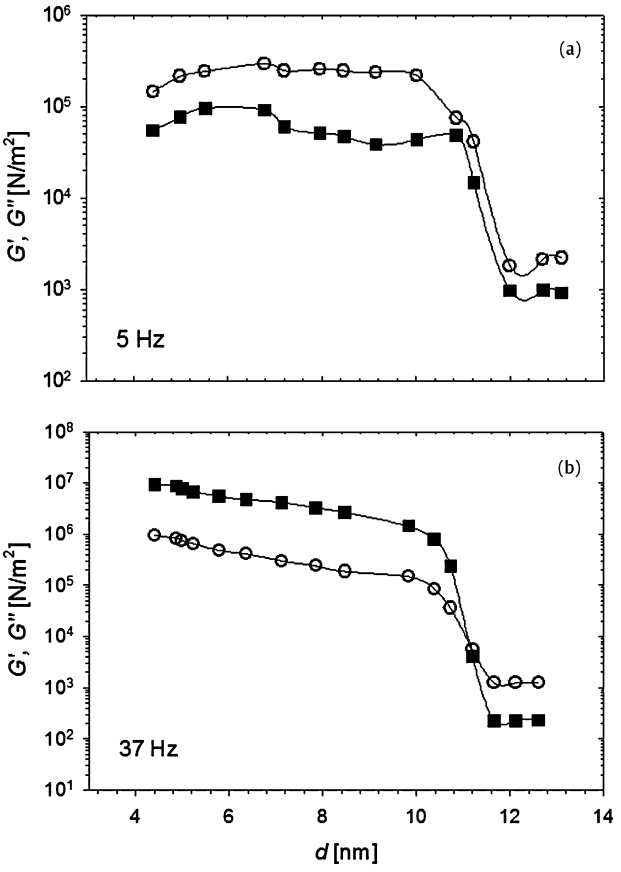

Fig. 5. Thickness dependence of the effective shear moduli measured at 5 Hz (panel a) and 37 Hz (panel b), for the same Brij 96 microemulsion characterized in Fig. 4. The logarithmic elastic modulus, $G'(\omega)$ (solid squares) and viscous modulus, $G''(\omega)$ (open circles) are plotted versus film thickness, d. The data were taken while the microemulsion sample was sheared in the SFA with amplitude <10 nm. No hysteresis was observed. Hydrophobic surfaces were employed, as described in the text.

shear displacement amplitudes greatly exceeded the film thickness, measurements were also made at much smaller amplitude, 1–10 nm, and the linear response as a function of oscillatory frequency was inspected. Typical results are shown in Fig. 4 at the same surface separation ($d = 4.4$ nm); the effective storage (G') and the loss (G'') moduli are plotted as a function of frequency. It

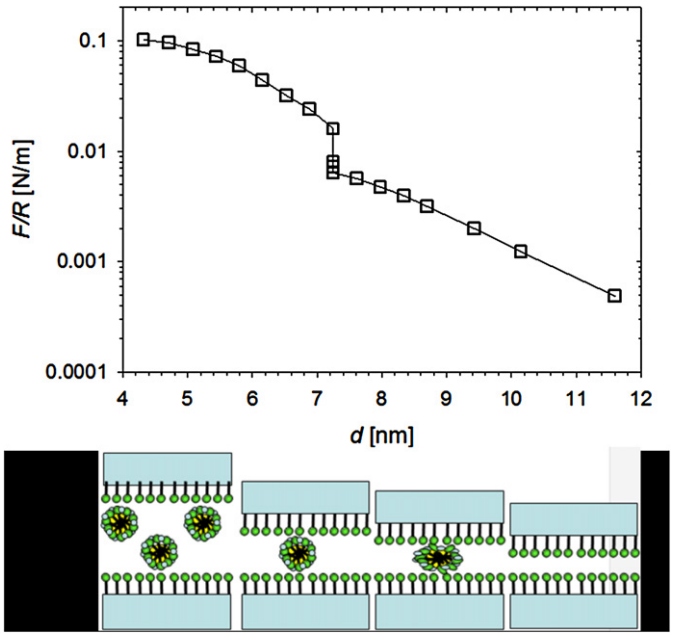

Fig. 6. Force–distance profile of the Brij microemulsion. Top panel: logarithmic force normalized by the radius of curvature of cylindrical lenses, $\log(F/R)$, is plotted against film thickness. Note that at a separation of about 7.2 nm, the film became stubborn to further displacement, and a very high load was required to squeeze the sample to a hard-wall contact; this explains the seeming discontinuity in the force–distance curve. Bottom panel: schematic diagram explaining the tentative picture that thin films in the range of thickness 13 to 7 nm are comprised of deformed micelles and that confinement to thinner films expels micelles with concomitant even more drastic structural deformation of the remaining micelles, until the thinnest films retain only adsorbed surfactant.

was found that at the lowest frequencies, viscous properties dominate and $G'' > G'$, but the converse held at frequencies above 7 Hz. Note that the viscous modulus G'' grew in direct proportion to frequency (slope of $\alpha = 1$ on the log–log plot), which implies a constant viscosity. When increasing the oscillatory amplitude to 150 nm, nonlinear responses of the kind summarized in Fig. 3 were recovered.

The dependence on thickness was considered in experiments where the films were compressed on the time scale of minutes to tens of minutes and the normal forces resisting compression were measured. No dependence on the approach rate was noticed. Plotted as a function of the film thickness d, Fig. 5 shows the linear response storage modulus (G') and the loss modulus (G'') as a function of film thickness but at constant oscillatory frequency. Fig. 5a refers to a frequency less than the crossover frequency, for which $G'' > G'$ for the thinnest films (cf. Fig. 4); Fig. 5b refers to the converse situation, a frequency at which $G' > G''$ for the thinnest films. In both cases, the shear moduli increase abruptly when films are squeezed to thickness 10–12 nm. A schematic diagram of the structural rearrangements, from which this might result, are sketched in Fig. 6b.

This transition thickness in the rheological response is strikingly close to the micelle size of 13 nm, measured independently by light scattering. The rheological perturbations when the microemulsion was squeezed into even thinner films appear to reflect structural reorganizations, possibly elongation of the micelles at first and ultimately its breakup at the thinnest film thicknesses. Note also that for the lower frequency (5 Hz), $G'' > G'$ regardless of thickness and that at the higher frequency (37 Hz), the converse held regardless of thickness, which is also consistent with the data in Fig. 4. The rheological data were collected while the two substrates were separated and approached in replicate at least 3 times for each sample. No hysteresis was found.

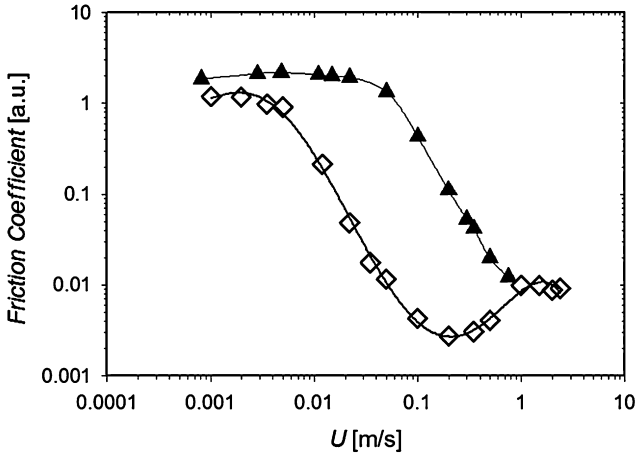

Fig. 7. Macroscopic friction coefficient, measured on a standard tribology (MTM) machine, plotted as a function of entrainment speed U for water (solid triangles) and microemulsion as the lubricant (open diamonds). The load was 1 N, equivalent to a pressure of 0.22 MPa, and the contact area between the rotating sphere and disk was of diameter 2.4 mm.

This same transition thickness was observed when the surfaces were brought together within the SFA in the absence of shear. The force, to compress the microemulsion to a given thickness, is plotted on a semilogarithmic scale in Fig. 6. It was monotonically repulsive starting at the spacing $d = 12$ nm; and was reversible upon approach and separation without adhesion. This number agrees well with the measured micelle size (∼13 nm), showing that the micelles display a measurable resistance to applied force. Note that below a separation of about 7.2 nm, the film became stubborn to further displacement; a very high load was required to squeeze the sample to a hard-wall contact. This explains the seeming discontinuity in the force–distance curve. Note also that the forces in these experiments were large, so large that the mica sheets deformed visually to become parallel, so that the customary cylindrical geometry was lost at the apex. Therefore it was appropriate to normalize the normal forces by the area of the flattened contacts, giving the normal pressure. This number was ≈1 MPa (12 nm thickness) and ≈10 MPa (4 nm thickness) but the data are too scattered to draw more quantitative conclusions than this.

A fascinating aspect of these hypothesized structural rearrangements, which influence so prominently the static normal forces, is that their influence on shear resistance was limited. Only a small feature can be observed around $d = 7.2$ nm in Fig. 5a (where viscous forces dominate) and no feature is observed in Fig. 5b (where elastic forces dominate).

3.3. Tribology of the conventional kind

Going beyond the idealized conditions of a surface forces experiment—a natural question was to inquire, what was tribology of this same system but experienced in a less idealized system? The tribological properties of the microemulsion were measured using a mini traction machine (MTM) with PDMS surfaces. A full Stribeck curve was obtained. Fig. 7 shows the friction coefficient μ plotted against the entrainment velocity U, for both the microemulsion and for deionized water. The three regimes of lubrication (boundary, mixed, and elastohydrodynamic) are easily distinguished. The boundary regime is observed for $U < 0.003$ m/s, where the friction coefficient is almost constant at a value of $\mu \approx 1$. In this regime, the lubricant is almost fully absent from the contact zone, so the PDMS substrates are in direct contact. The friction coefficient value for the microemulsion is just slightly smaller than that one for water in the boundary regime ($\mu_{water} \approx 2$), suggesting that some adsorbed species are present on the substrates, thus increasing slightly the lubricating properties of the microemulsion. The mixed regime is observed in the range of 0.003 m/s $< U < 0.2$ m/s. In this regime, more fluid is entrained in a contact area as U increased and friction is reduced. Full film lubrication is observed for $U > 0.2$ m/s, where the contact is in the elastohydrodynamic (EHL) regime. When increasing the speed, the friction coefficient increased to a second plateau ($\mu \approx 0.01$), which is simultaneously the minimum of EHL for water. However, this second plateau also corresponded to excessive foaming of the system in the tribometer.

4. Summary

This comparison of the tribology and rheology of a model microemulsion in the bulk phase and in nanometer-thin films confined between hydrophobic surfaces, is considered to be the first to date for a microemulsion. The main finding is the following. Whereas in the bulk, the microemulsion displays the anticipated constant viscosity over the entire range of measured shear rate, when the film thickness became less than the size of bulk micelles, the resistance to shear was enhanced by orders of magnitude.

A tentative schematic scenario to explain the resistance to compression is the following. First, spherical micelles are compressed in the presence of excess surfactant to a thickness equal to their unperturbed diameter; upon further compression to 7–12 nm thickness, the micelles are squeezed in the presence of a surfactant monolayer on each hydrophobic solid surface. While the nature of the reorganization at $d < 7$ nm is unclear, the ultimate state of losing micelles and simply being left with two surfactant monolayers in contact is consistent with the fact that the tribological behavior observed in this final state is so similar to that observed in our earlier study of adsorbed surfactants [7].

Contrasting now the differences between tribology experiments of the conventional kind, and the tribology between smooth surfaces in a surface forces apparatus, the biggest difference between the microemulsion and water behavior in the Stribeck curve is the minimum indicating the transition from the EHL to the mixed-lubrication regime. The minimum for microemulsion is shifted toward a lower value of speed U and shows a lower value of friction coefficient as well. Although the plot is evidently shifted, its slope in the mixed region is kept constant. As the bulk viscosity of the microemulsion is only twice that of water, this cannot be explained by a bulk effect and surely stems from altered surface properties. Tentatively, we attribute this to micelle/surfactant adsorption on the hydrophobic surfaces, effectively rendering them hydrophilic. Enhanced entrainment of the lubricant improves wetting conditions and affects the flow, as has been observed by the authors previously for aqueous solutions of another non-ionic surfactant family, the Tweens [7].

This study of an industrially-important mesostructure confined to the nano-scale illustrates the potential of nano-measurements in application to complex fluids encountered in everyday-life systems. Looking to the future, it is our hope that with further experimentation, similar measurements pursued in this spirit may aid in the design and formulation of products that carry immediate value-added impact on quality of life. However, the influence of the oil selected for the oil element of the microemulsion has not yet been addressed.

Acknowledgments

M.G. thanks Unilever Corporate Research (UK) for a postdoctoral fellowship. The authors are grateful to Janet Wong at the University of Illinois for many insightful discussions and suggestions. The authors are grateful for the advice and assistance of Asish Nandi (Unilever) when formulating the microemulsions.

This work was supported by a grant from Unilever Corporate Research (UK), using facilities supported by a grant to the University of Illinois from National Science Foundation, NSF-CMS-05-55820 and the NSF Nanoscience Engineering Initiative, NSF-DMR-0071761. Partial equipment support was also provided by Science and Technology Center for Purification of Water, NSF-CTS-0120978.

References

[1] M. Gradzielski, H. Hoffman, Rheological properties of microemulsions, in: P. Kumar, K.L. Mittal (Eds.), Handbook of Microemulsion Science and Technology, Marcel Dekker, New York, 1999, pp. 357–386.
[2] K. Krishnan, K. Almdal, W.R. Burghardt, T.P. Lodge, F. Bates, Phys. Rev. Lett. 87 (2001) 098301-1.
[3] K. Krishnan, W.R. Burghardt, T.P. Lodge, F. Bates, Langmuir 18 (2002) 9676.
[4] Ch.-M. Chen, G.G. Warr, J. Phys. Chem. 96 (1992) 9492.
[5] G.G. Warr, Colloids Surf. A Physicochem. Eng. Aspects 103 (1995) 273.
[6] M.R. Anklam, R.K. Prud'homme, G.G. Warr, AIChE J. 41 (1995) 677.
[7] M. Graca, J.H.H. Bongaerts, J.R. Stokes, S. Granick, J. Colloid Interface Sci. 315 (2007) 662.
[8] N.J. Kale, L.V. Allen, Int. J. Pharm. 57 (1989) 87.
[9] S. Tenjarla, Crit. Rev. Ther. Drug Carrier Syst. 16 (1999) 461.
[10] J. Flangan, H. Singh, Crit. Rev. Food Sci. Nutr. 46 (2006) 221.
[11] Y. Liu, K. Wolf, M.C. Messmer, Langmuir 17 (2001) 4329.
[12] A.Y. Fadeev, T.J. McCarthy, Langmuir 16 (2000) 7268.
[13] T. Vallant, J. Kattner, H. Brunner, U. Mayer, H. Hoffman, Langmuir 15 (1999) 5339.
[14] A. Ulman, Chem. Rev. 96 (1996) 1553.
[15] C.R. Kessel, S. Granick, Langmuir 7 (1991) 532.
[16] H.-W. Hu, S. Granick, Langmuir 10 (1994) 3857.
[17] J. Peanasky, H.M. Schneider, S. Granick, C.R. Kessel, Langmuir 11 (1995) 953.
[18] J.H.H. Bongaerts, K. Fourtouni, J. Stokes, Tribol. Int. 40 (2007) 1531.
[19] A.L. Demirel, S. Granick, J. Chem. Phys. 115 (2001) 1498.
[20] J. Peachey, J. Van Alsten, S. Granick, Rev. Sci. Inst. 62 (1991) 463.
[21] J. Israelachvili, J. Colloid Interface Sci. 44 (1973) 259.